PHYSICAL REVIEW B VOLUME 7, NUMBER 5 1 MARCH 1973

F^{19} Nuclear Acoustic Resonance in $RbMnF_3$ with K^+, Co^{++}, Ni^{++}, Fe^{++}, and Mg^{++} Impurities

R. L. Melcher

IBM Thomas J. Watson Research Center, Yorktown Heights, New York 10598

R. H. Plovnick*

Laboratory of Atomic and Solid State Physics, Cornell University, Ithaca, New York 14850

(Received 22 September 1972)

We report the results of an experimental study of the F^{19} nuclear-acoustic-resonance spectrum in the antiferromagnetic phase of $RbMnF_3$ doped with small amounts of K^+, Co^{++}, Ni^{++}, Fe^{++}, and Mg^{++} impurities. The results show that the only nuclear spins taking part in this process are those in the immediate vicinity of the impurity ions. Only because of the symmetry-breaking effect of the impurity ions is it possible to couple elastic waves to the F^{19} nuclear spins. The observed spectra show large qualitative variations depending on the particular type of impurity ion involved. Attempts at achieving a quantitative understanding of the spectra were not successful.

I. INTRODUCTION

In the original work on the F^{19} nuclear-acoustic-resonance (NAR) spectrum of $RbMnF_3$ in the antiferromagnetic phase[1] the conclusion was reached that the Silverstein[2] nuclear-spin–phonon interaction was operative. This coupling mechanism involves elastic waves coupling via the magnetoelastic interaction to the ordered electronic spins of the crystal. This magnetoelastic interaction causes the electronic spins to oscillate at the frequency of the driving elastic strain. As a consequence of the transferred hyperfine interaction[3] the oscillating electronic spins produce an oscillating internal magnetic field acting on the F^{19} nuclear spins. The resulting nuclear-spin–phonon interaction is a two-step process proceeding via the intermediary electronic-spin system. Merry *et al.*[4] have pointed out that the symmetry of the F^- ions (D_{4h}) in the ideal cubic perovskite structure of $RbMnF_3$ leads to a cancellation of the oscillating hyperfine field. Therefore this coupling mechanism vanishes in the perfect perovskite lattice. They suggest that the strong experimental evidence that the Silverstein mechanism was observed in the original experiments[1] (i.e., the temperature dependence of the interaction strength and the dependence of the interaction strength on the type of elastic wave used in the measurements) could be reconciled with the calculated null result if impurities or defects are introduced into the host crystal in order to lower the symmetry of the F^- sites. In this paper, we present the results of an experimental investigation into the effect of impurities on the F^{19} NAR spectrum in $RbMnF_3$. Our results on controlled samples of $RbMnF_3$ containing the order of 1 at.% of K^+, Co^{++}, Ni^{++}, Fe^{++}, or Mg^{++} basically substantiate the suggestion of Merry *et al.*[4] Since the F^{19} NAR [as opposed to the conventional nuclear-magnetic-resonance (NMR)] spectrum in $RbMnF_3$ is due only to those F^{19} nuclear spins in the neighborhood of a symmetry-breaking impurity or defect, the spectrum is a potentially useful tool for the determination of the local magnetic field at F^{19} sites near the impurities or defects. However, we were not successful in quantitatively interpreting the NAR spectrum.

II. THEORY

A. Equilibrium Properties of $RbMnF_3$

This material possesses the ideal cubic perovskite structure at room temperature and below. It orders with a simple two-sublattice antiferromagnetic structure at $T_N \simeq 83\,^\circ$K with the easy axes of sublattice alignment being the equivalent $\langle 111\rangle$ axes. The low anisotropy (the effective anisotropy field $H_A \simeq 4$ Oe at 4.2 °K) causes the equilibrium sublattice orientation to be strongly affected by the presence of external magnetic fields.[5,6] For a field applied along the $\langle 001\rangle$ axis, the distribution of antiferromagnetic-domain alignment along the equivalent $\langle 111\rangle$ axes is immaterial and one can, without loss of generality, assume that the sublattices lie in the $(1\bar{1}0)$ plane. In zero field, they are parallel and antiparallel, respectively, to the $\langle 111\rangle$ axis. As the field is increased, the antiferromagnetic vector $\vec{\alpha} = \frac{1}{2}(\vec{\alpha}_1 - \vec{\alpha}_2)$ rotates in the $(1\bar{1}0)$ plane in equilibrium from the $\langle 111\rangle$ axis at zero field to the $\langle 110\rangle$ axis for fields[5,6] $H_0 \geq H_c \equiv [4H_E H_A/3(1-\chi_\parallel \chi_\perp)]^{1/2}$. In these expressions $\vec{\alpha}_1$ and $\vec{\alpha}_2$ are unit vectors parallel to the direction of the two magnetic sublattices, H_E and H_A are the effective exchange and anisotropy fields, and $\chi_\parallel$ and $\chi_\perp$ are the parallel and perpendicular susceptibilities. The sublattices themselves cant slightly in the $(1\bar{1}0)$

plane from the $\langle 110\rangle$ and $\langle \bar{1}\bar{1}0\rangle$ axes by the angle $t \simeq H_0/2H_E$. All the experiments to be discussed in this study were performed to the high-field limit $H_0 > H_c$. Therefore, the equilibrium direction cosines for the two sublattices assuming no impurity-induced changes are

$$\vec{\alpha}_1^0 = (1/\sqrt{2},\ 1/\sqrt{2},\ \cos t), \tag{1a}$$

$$\vec{\alpha}_2^0 = (-1/\sqrt{2},\ -1/\sqrt{2},\ \cos t). \tag{1b}$$

For more general orientations of the external field the equilibrium behavior is more complex and can lead to inequivalent domains and metastable states. Although we shall present F^{19} NAR spectra for $\langle 110\rangle$ and $\langle 111\rangle$ field orientations, we will not analyze these in detail.

B. F^{19} Nuclear Magnetic Resonance

The F^{19} NMR has been extensively studied in the paramagnetic phase of a number of perovskite fluorides with the chemical formula ABF_3, where A is Rb^+, K^+, or Tl^+ and B is Mn^{++}, Fe^{++}, Co^{++}, or Ni^{++}.[3,7-18] In an external magnetic field there are in general three magnetically inequivalent F^{19} sites whose resonances are shifted from positions expected in diamagnetic materials because of the magnetic interaction between the F^{19} nuclear spin and the surrounding paramagnetic ions. These shifts are typically the order of a few percent of the external field and are proportional to the static susceptibility of the paramagnetic ions. They are a consequence of both the classical dipole interaction with the paramagnetic ions and the transferred hyperfine interaction with the $2s$ and $2p$ F^- orbitals.[3] Although the F^{19} resonance in the magnetically ordered phase has not been so extensively studied, existing measurements[19,20] on $RbMnF_3$ show that the above considerations are basically unchanged (this is not true for materials such as $KMnF_3$ whose symmetry is lowered by structural phase transitions). The symmetry of the F^{19} site (D_{4h}) ensures that even in the antiferromagnetic phase of $RbMnF_3$ the shifts of the F^{19} NMR lines are proportional to the bulk susceptibility.

Consider an external field applied along the $\langle 001\rangle$ (z) axis. There are two inequivalent F^{19} sites denoted by C and A with twice as many A sites as C sites. The line joining the two Mn^{++} nearest neighbors to the C site is parallel to the $\langle 001\rangle$ axis. For the A sites, this line is parallel to the equivalent $\langle 100\rangle$ and $\langle 010\rangle$ axes (see Ref. 12 for further description of these two sites). The Hamiltonians for spins at each of these two sites are

$$\mathcal{H}^C = -\gamma_N \hbar H_0 I_z^C + \sum_l A_{11}(l)[I_x^C \langle s_x(l)\rangle + I_y^C \langle s_y(l)\rangle] + A_{33}(l) I_z^C \langle s_z(l)\rangle \tag{2a}$$

and

$$\mathcal{H}^A = -\gamma_N \hbar H_0 I_z^A + \sum_l A_{11}(l)[I_x^A \langle s_x(l)\rangle + I_z^A \langle s_z(l)\rangle] + A_{33}(l) I_y^A \langle s_y(l)\rangle, \tag{2b}$$

where γ_N is the nuclear gyromagnetic ratio, H_0 is the magnitude of the external field, $A_{ii}(l)$ is the ii component of the magnetic-interaction tensor (including both the classical dipole and nearest-neighbor transferred hyperfine interactions) between the nuclear spin and the Mn^{++} ion on the lth lattice site. In the paramagnetic phase, $\langle s_x(l)\rangle = \langle s_y(l)\rangle = 0$. In the antiferromagnetic phase, $\langle s_x(l)\rangle = -\langle s_x(-l)\rangle$ and $\langle s_y(l)\rangle = -\langle s_y(-l)\rangle$, but $\langle s_z(l)\rangle = \langle s_z(-l)\rangle = \langle s_z\rangle$ (independent of l). Here, sites l and $-l$ are related by the inversion operator and $\langle\rangle$ denotes a thermal average. Therefore, the Hamiltonians for the two sites in both the paramagnetic and antiferromagnetic phases can be written

$$\mathcal{H}^C = -\gamma_N \hbar H_0 (1 + x^C) I_z^C, \tag{3a}$$

$$\mathcal{H}^A = -\gamma_N \hbar H_0 (1 + x^A) I_z^A. \tag{3b}$$

The relative shifts for a perfect crystal, x^C and x^A, are given by

$$x^C = -\frac{\sum_l A_{33}(l)}{\gamma_N \hbar H_0} \langle s_z\rangle = \frac{\sum_l A_{33}(l)}{\gamma_N \hbar N g \mu_B} \chi_m \tag{4a}$$

and

$$x^A = -\frac{\sum_l A_{11}(l)}{\gamma_N \hbar H_0} \langle s_z\rangle = \frac{\sum_l A_{11}(l)}{\gamma_N \hbar N g \mu_B} \chi_m. \tag{4b}$$

The molar susceptibility is given by χ_m, g is the electronic g factor, μ_B is the Bohr magneton, and N is Avogadro's number. Experimentally at $T = 77.4\ ^\circ K$ one finds $x^C = 0.049$ and $x^A = 0.030$ in $RbMnF_3$.[19]

C. Nuclear-Spin–Phonon Coupling

Silverstein[2] has proposed that nuclear spins in antiferromagnetic materials can interact with elastic waves (acoustic phonons) via a two-step process. The phonons interact directly via the magnetoelastic interaction[20,21] with the order electronic spins causing them to oscillate at the phonon frequency. (This assumes that the phonon frequency is much less than the spin-wave frequency as is the case for the present experiments. For a situation for which this is not true see Refs. 22 and 23.) Because of the hyperfine interaction between the electronic- and nuclear-spin systems, the oscillating electronic magnetization produces an oscillating component of the hyperfine field which, acting through the magnetic dipole interaction, can induce nuclear-spin transitions.

The magnetoelastic interaction for longitudinal elastic strain e_{xx} propagating along the $\langle 100\rangle$ (x) axis in $RbMnF_3$ is given by [21,24]

$$\mathcal{H}_{ME} = B_1(\alpha_{1x}^2 + \alpha_{2x}^2) e_{xx} + B_3 \alpha_{1x}\alpha_{2x} e_{xx}, \tag{5}$$

where B_1 and B_3 are coupling constants, and α_{1x} and α_{2x} are the direction cosines of the two magnetic sublattices with respect to the $x(\langle 100\rangle)$ axis. For a $\langle 001\rangle$ applied field $H_0 > H_c$, we have $\alpha_{1x} = \alpha_{1x}^0 + \bar{\alpha}_{1x}$ and $\alpha_{2x} = \alpha_{2x}^0 + \bar{\alpha}_{2x}$, with $\bar{\alpha}_{1x}$, $\bar{\alpha}_{2x} \ll 1$ and $\alpha_{1x}^0 = 1/\sqrt{2}$ and $\alpha_{2x}^0 = -1/\sqrt{2}$ [Eqs. (1)]. To second order in small quantities the magnetoelastic interaction can be written

$$\mathcal{H}_{\mathrm{ME}} = b_1(\bar{\alpha}_{1x} - \bar{\alpha}_{2x})e_{xx}\,. \tag{6}$$

The effective magnetoelastic fields acting on the two sublattices are therefore

$$H_{1x}^{\mathrm{ME}} = -\frac{1}{M_0}\frac{\partial \mathcal{H}_{\mathrm{ME}}}{\partial \bar{\alpha}_{1x}} = -\frac{b_1}{M_0}\,e_{xx}\,, \tag{7a}$$

$$H_{2x}^{\mathrm{ME}} = -\frac{1}{M_0}\frac{\partial \mathcal{H}_{\mathrm{ME}}}{\partial \bar{\alpha}_{2x}} = \frac{b_1}{M_0}\,e_{xx} = -H_{1x}^{\mathrm{ME}}\,, \tag{7b}$$

where M_0 is the magnitude of the sublattice magnetization and $b_1 = (\sqrt{2})(B_1 - \frac{1}{2}B_3)$. The fact that $RbMnF_3$ is not piezomagnetic requires that $\vec{H}_1^{\mathrm{ME}} = -\vec{H}_2^{\mathrm{ME}}$, as given in Eq. (7b). This result [Eqs. (7)] has the important consequence that the magnetoelastic interaction causes each of the two magnetic sublattice vectors $\vec{M}_i \equiv \vec{M}_0\alpha_i$ $(i = 1, 2)$ to rotate rigidly and with the same sense about the z ($\langle 001\rangle$) axis. This rotation does not invalidate the symmetry arguments used in deriving Eqs. (3) above. Therefore, we see that because of the high symmetry of the F^- site, there is no alternating-magnetic hyperfine interaction acting on the F^{19} nuclei due to the presence of this elastic strain. Thus, the Silverstein nuclear-spin–phonon interaction vanishes. This same result has been obtained in Ref. 4 by a more formal calculation.

D. Symmetry Breaking by Impurities

Merry *et al.*[4] have pointed out that the introduction of lattice defects (impurities, vacancies, dislocations, etc.) lowers the local symmetry of the F^- sites surrounding the impurities, thereby invalidating the arguments of the previous paragraphs. Defects not only alter the diagonal part of the Hamiltonian leading to new values of x^A and x^C for the surrounding F^{19} nuclei; they also lead to off-diagonal terms which have the effect of producing nonzero hyperfine fields in the xy ($\langle 001\rangle$) plane. The magnetoelastically induced oscillation of the sublattice magnetization can then lead to a nonzero oscillating hyperfine field acting on the F^{19} nuclei. The two primary effects of impurities on the resonance behavior of the surrounding F^{19} nuclear spins are to alter their resonance field and lead to a nonzero nuclear-spin–phonon interaction.

The symmetry of the F^- site can be broken in two different ways. The introduction of a monovalent alkali ion such as K^+ to replace some of the Rb^+ will presumably lead to a local distortion of the MnF_6^{-3} octahedra with an attendant lowering of the F^--site symmetry from D_{4h} to perhaps C_{2v} or C_{4v}. The introduction of vacancies or divalent substitutions for Mn^{++} (e.g., Co^{++}, Ni^{++}, Fe^{++}, or Mg^{++}) will lower the magnetic symmetry of the surrounding F^- sites by virtue of changes in $A_{ii}(l)$ and $\langle \vec{s}(l)\rangle$. Results due to both types of impurities are reported in this paper.

To a first approximation monovalent impurities will affect only nearest-neighbor F^{19} nuclear spins. The nearest-neighbor Mn^{++}-F^{19} transferred-hyperfine-interaction constants in $RbMnF_3$[12] and $KMnF_3$[3] are equal to within the experimental error and almost isotropic [e.g., $A_{11}^{\mathrm{hyp}}(l) \simeq A_{33}^{\mathrm{hyp}}(l)$]. Therefore, the primary effect of K^+ impurities is expected to arise from the dipole interaction evaluated at the low-symmetry-distorted F^- site. On the other hand, the contribution of the divalent-impurity–F^{19} hyperfine interaction to $A_{ii}(l)$ is sufficiently different for the various impurities considered[7–18] compared to the Mn^{++}-F^{19} hyperfine interaction that nearest-neighbor F^{19} nuclear spins will have their resonances shifted completely out of the range of the observed spectra. Second, third, etc., nearest neighbors are relatively unaffected by the short-range hyperfine interaction and therefore will feel only the change in the classical dipole field due to the impurity. The resulting change in the values for x^A and x^C, etc., due to the dipole interaction may be as much as a factor of 2.

III. EXPERIMENTAL

(i) The single-crystal samples used in these experiments were cut from Czochalski-grown boules. The melt was prepared using two different processes similar to those described by Plovnick and Camobreco for the growth of "pure" crystals.[25] The Fe^{++}, Mg^{++}, Co^{++}, and one of the Ni^{++} doped samples were prepared from binary fluorides. The K^+ and one Ni^{++} doped samples were prepared from carbonates.[25] The concentration of impurities intentionally introduced into the melt was determined by atomic-absorption spectroscopy and flame-emission and neutron-activation analysis. After cutting and polishing, gold-on-chromium electrodes were deposited on $\langle 100\rangle$ faces of the samples, which were in the form of ~1-cm cubes.

(ii) All measurements reported here were performed with the samples immersed in liquid nitrogen ($T = 77.4\,^{\circ}\mathrm{K}$). The continuous-wave ultrasonic transmission spectrometer used was similar to that described by Melcher *et al.*[26] However, to achieve better impedance matching to the transducer-sample-transducer resonator the matching networks (variable series inductors) were located in the nitrogen bath physically near the sample.

(iii) The magnetic field was calibrated using the proton nuclear magnetic resonance in mineral oil.

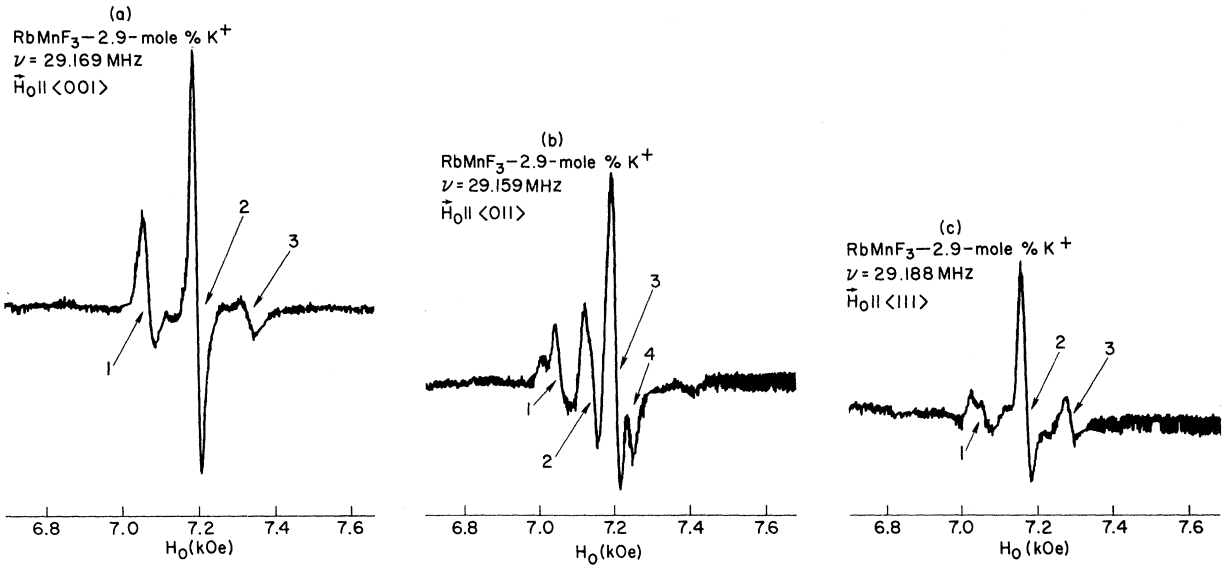

FIG. 1. F^{19} NAR absorption spectrum for $RbMnF_3$: 2.9 mole% K^+. T=77.4 °K, e_{xx} strain ($\vec{k}_{long} \parallel \langle 100 \rangle$). (a) $\vec{H}_0 \parallel \langle 001 \rangle$, (b) $\vec{H}_0 \parallel \langle 011 \rangle$, (c) $\vec{H}_0 \parallel \langle 111 \rangle$.

The attendant errors in determining line positions are much less than the error resulting from asymmetric and overlapping resonance lines.

IV. EXPERIMENTAL RESULTS

The primary experimental data are in the form of ultrasonic attenuation at fixed frequency versus magnetic field in the neighborhood of the F^{19} nuclear-resonance field for each of the several samples studied here. Because of the phase-sensitive detection used, the actual spectra correspond to the first derivative of the absorption signal. It should be emphasized that the spectrometer (as used here) is sensitive only to absorption. Figures 1–5 show recorder tracings of the observed spectra. Shown in these figures are the spectra for ⟨001⟩ and in some cases ⟨110⟩ and ⟨111⟩ applied fields. As discussed in Sec. II A, all possible antiferromagnetic domains are equivalent for a ⟨001⟩ field but not necessarily for other field orientations. For this

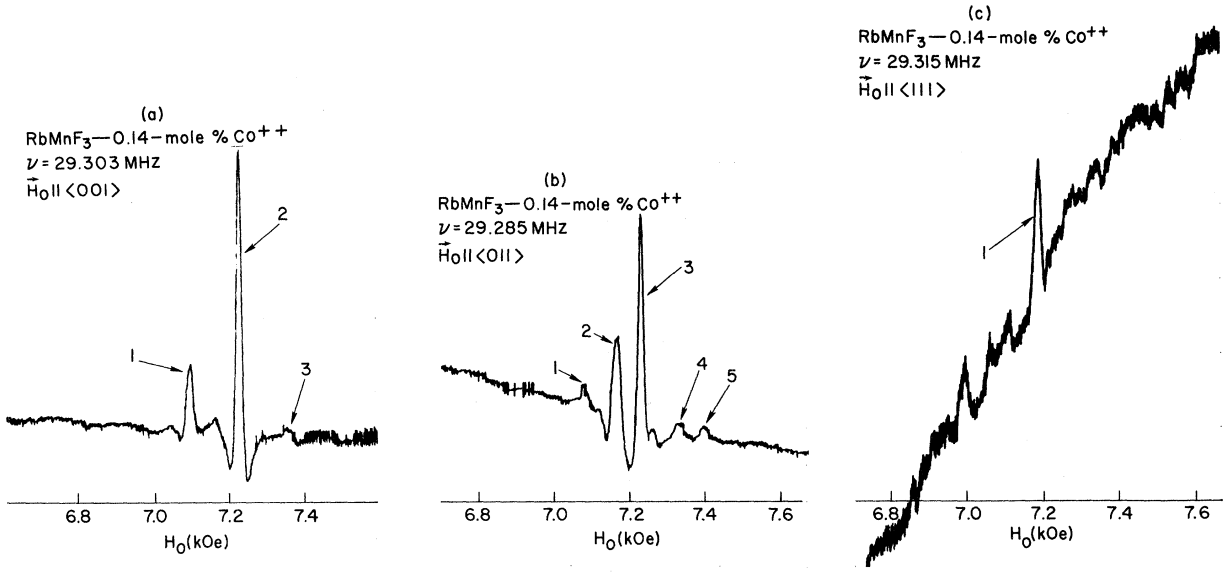

FIG. 2. F^{19} NAR absorption spectrum for $RbMnF_3$: 0.14 mole% Co^{++}. T=77.4 °K, e_{xx} strain ($\vec{k}_{long} \parallel \langle 100 \rangle$). (a) $\vec{H}_0 \parallel \langle 001 \rangle$, (b) $\vec{H}_0 \parallel \langle 011 \rangle$, (c) $\vec{H}_0 \parallel \langle 111 \rangle$.

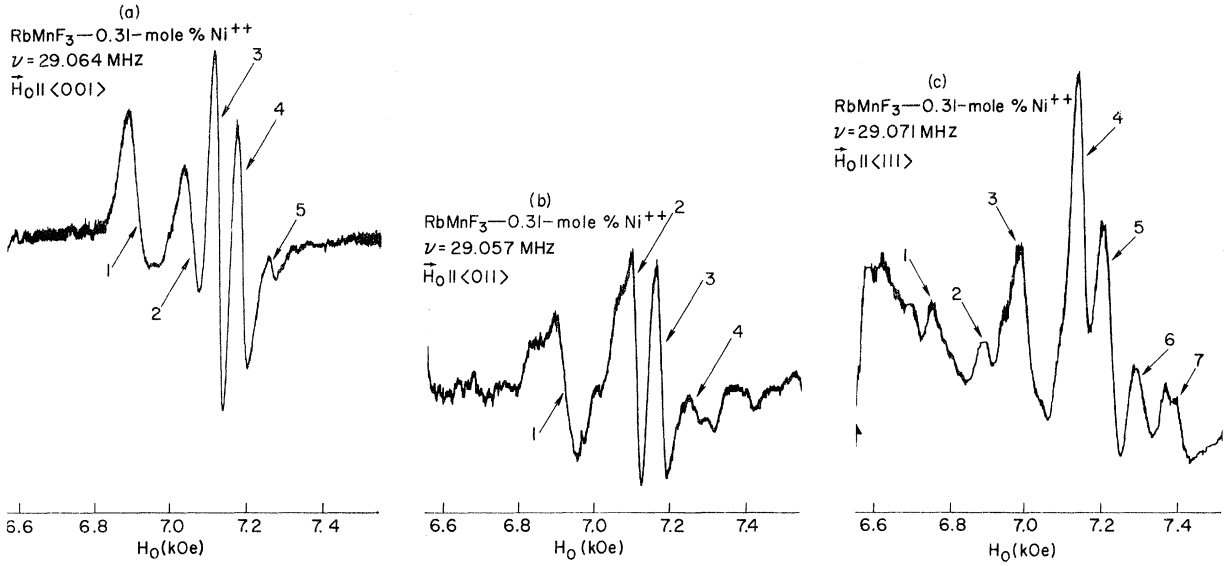

FIG. 3. F^{19} NAR absorption spectrum for $RbMnF_3$: 0.31 mole% Ni^{++}. Crystal grown from a melt prepared from binary fluorides as discussed in Ref. 25. $T = 77.4\,^{\circ}K$, e_{xx} strain ($\vec{k}_{long} \| \langle 100 \rangle$). (a) $\vec{H}_0 \| \langle 001 \rangle$, (b) $\vec{H}_0 \| \langle 011 \rangle$, (c) $\vec{H}_0 \| \langle 111 \rangle$.

reason, the discussion below is restricted primarily to the $\langle 001 \rangle$ field orientation.

In Table I the data are analyzed in terms of the line position (value of x), the linewidth (peak to peak of the absorption derivative), and intensity (the peak value of the ultrasonic attenuation resulting from the nuclear-spin–phonon coupling). Also given is the off-resonance background attenuation which is dominated by the linear magnetoelastic coupling[21] to the antiferromagnetically ordered electronic-spin system [Eq. (6)].

Although the effects of the individual impurities are to be discussed below, several general comments concerning the spectra can be made. (i) The qualitative form of the spectra, i.e., the number of lines, their width, their intensity, etc., is dramatically influenced by the type of impurity. (ii) Both magnetic and nonmagnetic impurities in-

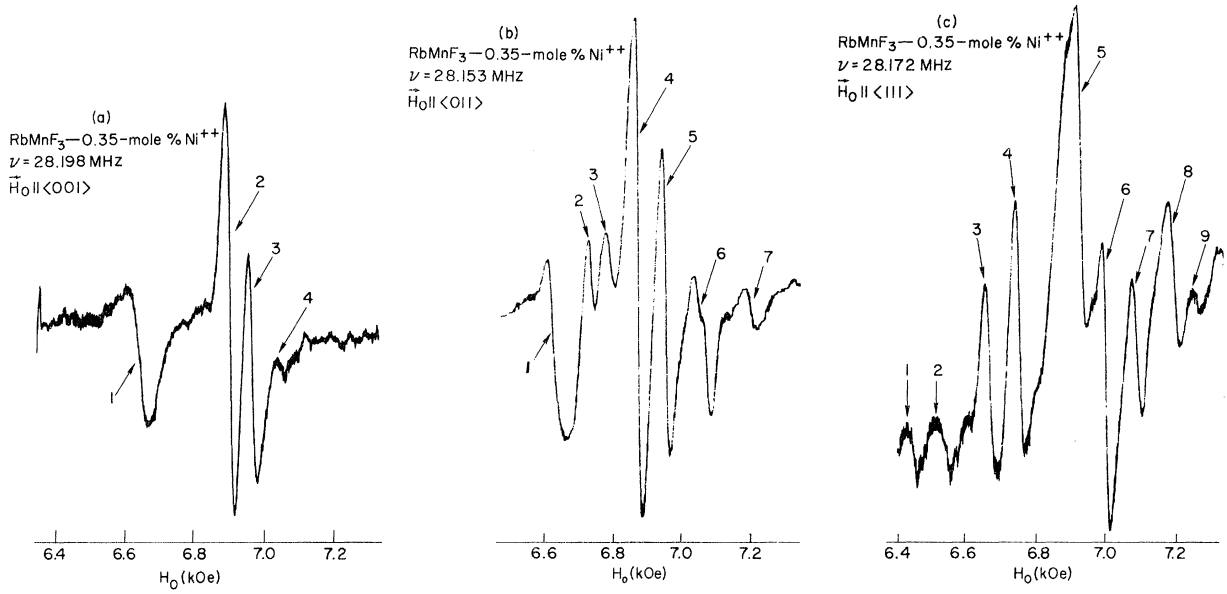

FIG. 4. Same as Fig. 3 except crystal contains 0.35 mole% Ni^{++} and the melt was prepared from carbonates as discussed in Ref. 25.

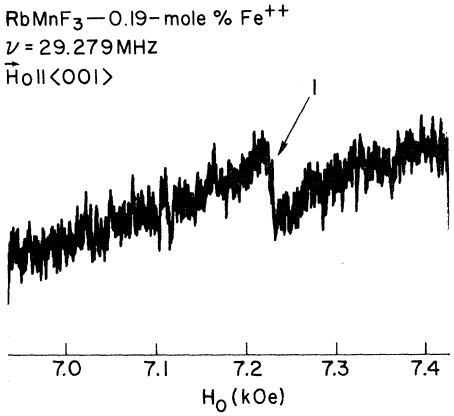

FIG. 5. F^{19} NAR absorption spectrum for $RbMnF_3$: 0.19 mole% Fe^{++}. $T = 77.4$ °K, e_{xx} strain ($\vec{k}_{long} \parallel \langle 100 \rangle$). $\vec{H}_0 \parallel \langle 001 \rangle$.

fluence the spectra. (iii) The magnetoelastic properties are dominated in some samples by small amounts of impurities. This is evidenced by the order-of-magnitude variation in the background attenuation for the different samples at $T = 77.4$ °K and $\vec{H}_0 \parallel \langle 001 \rangle$. For $T > T_N$, the background attenuation of all the samples was equal to within a factor of 2. (iv) There is some correlation between the magnitude of the background attenuation α_0 and the peak nuclear-spin attenuation $\Delta\alpha_n$. This is an indication that the nuclear spins are coupled to the elastic strain via the intermediate magnetoelastic oscillations of the electronic spins.

A. $RbMnF_3 : K^+$

Because of the relative ionic sizes the substitution of K^+ for Rb^+ is assumed to cause a local distortion of the ideal cubic structure of $RbMnF_3$, lowering the symmetry of the neighboring F^- sites. $KMnF_3$, which is isomorphous to $RbMnF_3$ at room temperature, undergoes a purely structural phase transition at $T_c \simeq 185$ °K,[27,28] and further structural changes at its magnetic transitions at $T_{N1} \simeq 88$ °K and $T_{N2} \simeq 82$ °K.[29] The main distortion at the 185 °K transition is a rotation of the MnF_6^{-3} octahedra about the cubic axes with adjacent octahedra rotating in opposite directions.[28] This distortion lowers the F^--site symmetry from D_{4h} to C_{2v}. On the basis of a similar local distortion of the nearest-neighbor F^- sites to a K^+ impurity in $RbMnF_3$ we have attempted a calculation of the dipole fields at the new (low-symmetry) F^- sites. For MnF_6^{-3} rotation about the $\langle 001 \rangle$ axis the field at the C-type sites is unchanged, while that at the A-type sites is unchanged in the z direction but has nonvanishing components in the xy plane. Thus, the A sites have a nonvanishing spin-phonon interaction and the resonance field is unshifted from the bulk value. The coupling for the C sites still vanishes. The expected spectrum on this simple model is a single line with $x = 0.030$. The observed spectrum consists of three lines (see Fig. 1 and Table I), the most intense having $x = 0.030$ (the bulk x^A values), with weaker lines having $x = 0.048$ (the bulk x^C value) and $x = 0.009$. Apparently a more elaborate model is needed to understand this entire spectrum. In particular, other types of distortions around the impurity ion could be envisioned.

B. $RbMnF_3 : Co^{++}$

It is well established that the introduction of small amounts of Co^{++} (greater than 0.034 mole%) into $RbMnF_3$ changes the sign of the magnetic anisotropy constant so that the easy axes of antiferromagnetic alignment are no longer the $\langle 111 \rangle$ axes but rather the $\langle 100 \rangle$ axes.[6] Because of the strong Co^{++}-Mn^{++} and Mn^{++}-Mn^{++} exchange the Co^{++} impurities pin the magnetic sublattices in the preferred orientation of the Co^{++} ion. In the presence of a strong ($H_0 > H_c$) field along the $\langle 001 \rangle$ axis the sublattice equilibrium orientations are the $\langle 100 \rangle$ and $\langle 001 \rangle$ directions.[6]

The two samples studied here (0.28 and 0.14 mole%, respectively) gave equivalent results. They contain an order of magnitude greater Co^{++} than required to change the sign of the anisotropy. Therefore, the sublattices must be assumed to have the above orientations in the present experiments. However, for these sublattice orientations one can readily show that the linear magnetoelastic coupling vanishes for an e_{xx} strain. This result is, however, completely in disagreement with the very strong background absorption measured in the Co^{++} doped samples and the strong nuclear-spin–phonon attenuation measured (see Fig. 2 and Table I). Clearly more must be understood about the effect of Co^{++} impurities in $RbMnF_3$ before a detailed analysis of the NAR spectra can be attempted.

Ignoring these rather fundamental difficulties, we note that the $\langle 001 \rangle$ NAR spectrum in the Co^{++} doped samples consists of two dominant lines with $x = 0.030$ and $x = 0.049$, in agreement with the bulk values obtained by NMR for A- and C- type sites, respectively. The observed line shape (Fig. 2) has the general shape expected of an almost pure dispersion derivative. It is a fairly general result that an observed absorption signal contains contributions from the real as well as the imaginary part of the susceptibility whenever the coupling mechanism proceeds via an intermediate system which itself exhibits strong damping. The high background attenuation in the Co^{++} doped samples is evidence for the high damping of the intermediate electronic-spin system. In the K^+ doped samples discussed

in Sec. IV A the low background attenuation indicates lower electronic-spin damping, and the observed NAR spectrum more nearly corresponds to the imaginary part of the susceptibility. Similar effects have been discussed with regard to the NMR of nuclei in ferromagnetic materials.[30]

TABLE I. Summary of F^{19} NAR spectra.[a]

	Magnetic field orientation	α_0[b] (10^{-2} cm^{-1})	F^{19} NAR line[f]	Position[c] ($10^2 x$)	Width[d] (Oe)	Peak NAR attenuation[e] $\Delta\alpha_N$ (10^{-3} cm^{-1})
$RbMnF_3$: 2.9 mole% K^+	⟨001⟩	5.1	1	4.8±0.1	29±3	150
			2	3.0±0.1	19±4	360
			3	0.9±0.1	30±6	40
	⟨011⟩	6.1	1	5.2±0.1		110
			2	3.9±0.1		180
			3	3.0±0.1	22±3	415
			4	2.5±0.2		46
	⟨111⟩	7.3	1	5.54±0.1	39±15	100
			2	3.6±0.1	27±5	380
			3	2.0±0.1	23±10	68
$RbMnF_3$: 0.14 mole% Co^{++}	⟨001⟩	16.2	1	4.9±0.1	40±10	520
			2	3.0±0.1	40±10	2200
			3	1.1±0.1		110
	⟨011⟩	19.1	1	5.2±0.1		135
			2	3.9±0.1	45±15	1100
			3	3.0±0.1	40±15	1870
			4	1.6±0.1		135
			5	0.7±0.1		112
	⟨111⟩	7.4	1	3.6±0.1	22±7	710
$RbMnF_3$: 0.31 mole% Ni^{++}	⟨001⟩	2.0	1	6.9±0.1	56±7	36
			2	4.8±0.1	40±5	20
			3	3.7±0.1	31±4	49
			4	2.8±0.1	34±5	33
			5	1.7±0.1	22±15	2
	⟨011⟩	3.2	1	6.7±0.2	54±10	27
			2	3.9±0.1	28±4	19
			3	2.9±0.1	34±5	21
			4	1.2±0.1	45±15	5.5
	⟨111⟩	3.9	1	7.3±0.2	28±6	10
			2	6.4±0.2	28±8	5.5
			3	5.6±0.3	60±30	59
			4	3.4±0.1	37±8	91
			5	2.4±0.1	43±8	64
			6	1.24±0.1	31±5	20
			7	0±0.1	45±15	44
$RbMnF_3$: 0.35 mole% Ni^{++}	⟨001⟩	2.2	1	8.15±0.1	65±10	22
			2	3.8±0.1	38±5	39
			3	3.0±0.1	31±6	17
			4	1.7±0.1	35±10	1
	⟨011⟩	1.9	1	8.2±0.1	58±8	48
			2	6.36±0.1	20±6	6
			3	5.5±0.1	27±8	6
			4	4.2±0.1	38±4	87
			5	3.0±0.1	35±4	49
			6	1.3±0.15	54±15	35
			7	−0.5±0.2	35±10	5.6
	⟨111⟩	2.3	1	11.2±0.2	38±8	7.3
			2	9.7±0.1	45±10	9.9
			3	7.5±0.1	38±6	30
			4	6.2±0.1	38±6	40
			5	3.5±0.1	38±4	52
			6	2.4±0.1	35±5	44
			7	1.2±0.1	35±5	20
			8	−0.4±0.1	35±5	21
			9	−1.3±0.1	23±6	1.6

TABLE I. (*Continued*)

	Magnetic field orientation	α_0[b] (10^{-2} cm^{-1})	F^{19} NAR line[c]	Position[d] ($10^2 x$)	Width[e] (Oe)	Peak NAR attenuation[f] $\Delta\alpha_N$ (10^{-8} cm^{-1})
$RbMnF_3$:	⟨001⟩	3.8	1	2.9 ± 0.1	27 ± 8	9.8
0.19 mole% Fe^{++}	⟨011⟩	5.6	1	4.0 ± 0.1		6.7
			2	3.0 ± 0.1	28 ± 8	16
	⟨111⟩	6.2	1	3.5 ± 0.1	30 ± 10	20
$RbMnF_3$:	⟨001⟩	2.0	1	2.8 ± 0.2	45 ± 15	5.3
0.6 mole% Mg^{++}						

[a]All data were obtained using ⟨100⟩ propagating longitudinal waves at a nominal frequency of 29 MHz. The actual numbers in this table were taken from much-expanded recorder traces of the spectra shown in Figs. 1–5.

[b]α_0 was determined from the width of the mechanical resonances of the crystal.

[c]See Eqs. (3) for a definition of the relative shift x of a given line. The errors quoted here are determined by the asymmetric and overlapping lines.

[d]Errors are determined by the overlapping and asymmetric lines.

[e]The absolute values of $\Delta\alpha_N$ are probably not accurate to better than 50%. The relative values for the different lines of a given sample and field orientation are accurate to approximately 15%.

[f]Line designations are noted in Figs. 1–5.

C. $RbMnF_3 : Ni^{++}$

The observed F^{19} NAR spectrum for the Ni^{++} doped samples (Figs. 3 and 4) consist of many lines, and are not entirely equivalent for nominally equivalent samples. The data shown in Fig. 3 were obtained on a sample prepared from binary fluorides, whereas the data in Fig. 4 are from a sample prepared from carbonates.[25] The qualitative difference in the F^{19} NAR spectra from the two samples is puzzling. It may be related to other impurities in the starting material, although we have no evidence that this is indeed the case.

In analyzing the data, it is possible to completely ignore the F^- sites which are nearest neighbors to the Ni^{++} impurities, since the hyperfine interaction constants Ni^{++}-F^{19} and Mn^{++}-F^{19} are sufficiently different[12,13] so as to shift the nearest-neighbor resonances out of the observed range. Since the Ni^{++}-Mn^{++} exchange constant is some 3.5 times the Mn^{++}-Mn^{++} exchange,[30,31] the main effect on the second- and third-nearest-neighbor F^{19} nuclear spins is expected to be the larger magnetic dipole moment existing at the impurity site. We have calculated the effect of the impurity dipole field on the 30 F^{19} second and third nearest neighbors in the presence of a large ⟨001⟩ external field. Of the 16 type-A next-nearest-neighbor (nnn) sites, eight are unshifted in field, four are shifted up by $+\Delta x$, and four are shifted down by $-\Delta x$. Of the eight type-C nnn sites, four are shifted up by $+\Delta x$ and four down by $-\Delta x$. The six third nearest neighbors (four type-A sites and two type-C sites) are unshifted by the impurity ion. The expected spectrum for up to and including the third nearest neighbors consists of six distinct lines. (Note that Δx is proportional to the difference in the Mn^{++} and Ni^{++} magnetic dipole moments.) Examination of Figs. 3 and 4 for a ⟨001⟩ field shows either four or five lines, depending upon the sample studied. Attempts at estimating the expected intensities did not significantly aid in comparing the theoretical and experimental spectra. {The relative intensity is estimated from the number of nuclei contributing to a given line and the square of the component of the dipole field in the xy [(001)] plane.}

This dipole impurity model is quite an oversimplification of the real situation. In particular, neither nonlinear-concentration effects nor lattice distortions have been considered. However, it is somewhat surprising that at least qualitative agreement cannot be obtained on this basis. Of course, our knowledge concerning Ni^{++} doped samples is very limited, since we do not really even know the sign of the resultant magnetic anisotropy constant.

D. $RbMnF_3 : Fe^{++}$

The very weak F^{19} NAR spectrum in Fe^{++}-doped $RbMnF_3$ was barely extractable from the noise (Fig. 5). The Fe^{++}-Mn^{++} exchange[32] is comparable to the Mn^{++}-Mn^{++} exchange, and therefore the change in the local dipole field is small compared to that resulting from Ni^{++} impurities. The only clearly discernible F^{19} NAR line for a ⟨001⟩ field has $x = 0.029$, which to within the experimental error is that expected for A-type sites in the bulk crystal. It may be significant that by far the most intense line expected on the basis of the second- and third-nearest-neighbor dipole calculation (see Sec. IVC) is that due to unshifted A-type nuclear sites. However, the limited data for the Fe^{++} impurities and limited agreement for the case of Ni^{++} impurities do not encourage us to draw any firm conclusions.

E. $RbMnF_3 : Mg^{++}$

This case corresponds most nearly to the case of a vacancy, since Mg^{++} has no uncompensated di-

pole moment. In principle, the explicit calculation of Merry *et al.*[4] should apply to this case. The observed resonance (not shown here) is, however, too weak to distinguish more than one unshifted (A-type) line and quantitative comparisons are difficult. However, contrary to the present experimental observations, the F^{19} NAR in the vicinity of a vacancy was calculated in Ref. 4 to be readily observable.

F. "Pure" $RbMnF_3$

The F^{19} NAR spectra obtained from a doubly grown boule of $RbMnF_3$ consisted of two lines with an intensity approximately the same as that obtained in Fe^{++} or Mg^{++} doped samples. These lines may result from unintentional trace impurities or from lattice defects. The sample used in the original observation of the F^{19} NAR in $RbMnF_3$[1] (grown by Stevenson by the Bridgman technique) was rerun on the present apparatus. The spectrum was essentially identical to that reported previously. The intensity of the spectrum from this sample is comparable to that observed in the Co^{++} doped samples discussed in Sec. IV B. Since chemical analysis revealed only trace impurities (the analysis was recently repeated with similar results), the difference between these two "pure" samples is remarkable. This may be due to growth-induced defects in the Bridgman-grown sample as assumed in Ref. 4. Etch-pit analyses[25] on the present two nominally pure Bridgman- and Czochalski-grown samples show less than a factor-of-2 difference in the dislocation density ($\sim 5\times10^5$ cm^{-2}). The possibility of growth- or magnetostrictively induced strains in "pure" $RbMnF_3$ should not be ignored, since these most likely would lower the F^--site symmetry. However, to our knowledge no quantitative data are yet available.

V. CONCLUSIONS

In spite of the lack of a quantitative description of the observed F^{19} NAR spectra in the impurity-doped samples of $RbMnF_3$, several conclusions can be reached. (i) In agreement with the simple calculation presented in Sec. II, and the more detailed analysis of Ref. 4, the Silverstein nuclear-spin–phonon interaction vanishes for the F^{19} nuclear spins in a perfect crystal of $RbMnF_3$. (ii) The introduction of impurities lowers the symmetry of the F^- site, leading to a nonvanishing spin-phonon interaction and to shifts in the resonances of the F^{19} nuclear spins in the neighborhood of impurities. (iii) Different types of impurities have vastly different effects on the NAR spectrum. Together with a quantitative theory the F^{19} NAR should in principle be a valuable technique for studying impurity states in $RbMnF_3$. (iv) The comparison between the nominally pure Czochalski- and Bridgman-grown samples shows that the NAR spectrum is quite sensitive to an additional, and as yet undetermined, structural parameter.

The present frequencies are small compared to the electronic-spin modes of the system (both pure and impurity modes). Therefore, the experiments are essentially static with respect to the electronic spins. A better understanding of the static properties of impurities in $RbMnF_3$ is essential to a quantitative understanding of the NAR spectra reported here.

ACKNOWLEDGMENT

We are indebted to J. Cozzo for technical assistance in carrying out these experiments.

*Present address: 3M Company, 3M Center, St. Paul, Minn. 55101.

[1] R. L. Melcher and D. I. Bolef, Phys. Rev. **184,** 556 (1969).
[2] S. D. Silverstein, Phys. Rev. **132,** 997 (1963).
[3] R. G. Shulman and K. Knox, Phys. Rev. **119**, 94 (1960).
[4] J. B. Merry, P. A. Fedders, and D. I. Bolef, Phys. Rev. B **5,** 3506 (1972).
[5] P. H. Cole and W. J. Ince, Phys. Rev. **150,** 377 (1966).
[6] W. J. Ince, D. Gabbe, and A. Linz, Phys. Rev. **185,** 482 (1969).
[7] R. G. Shulman and K. Knox, J. Chem. Phys. **42,** 813 (1965).
[8] R. E. Payne, R. A. Forman, A. H. Kahn, J. Chem. Phys. **42,** 3806 (1965).
[9] M. P. Petrov, Fiz. Tverd. Tela **7,** 1663 (1965) [Sov. Phys.-Solid State **7,** 1348 (1965)].
[10] M. P. Petrov and G. A. Smolenskii, Fiz. Tverd. Tela **7,** 2156 (1965) [Sov. Phys.-Solid State **7,** 1735 (1966)].
[11] M. P. Petrov, G. A. Smolenskii, and P. P. Syrnikov, Fiz. Tverd. Tela **7,** 3689 (1965) [Sov. Phys.-Solid State **7,** 2984 (1966)].
[12] M. B. Walker and R. W. H. Stevenson, Proc. Phys. Soc. Lond. **87,** 35 (1966).
[13] M. P. Petrov and G. A. Smolenskii, Zh. Eksp. Teor. Fiz. **50,** 871 (1966) [Sov. Phys.-JETP **23,** 579 (1966)].
[14] M. P. Petrov and V. A. Kudryashov, Fiz. Tverd. Tela **8,** 3124 (1966) [Sov. Phys.-Solid State **8,** 2503 (1967)].
[15] K. Hirakawa and S. Kadota, J. Phys. Soc. Jap. **23,** 756 (1967).
[16] M. P. Petrov, V. R. Korneev, and P. P. Sirnikov, Phys. Lett. A **28,** 618 (1969).
[17] M. P. Petrov, Zh. Eksp. Teor. Fiz. **56,** 1823 (1969) [Sov. Phys.-JETP **29,** 979 (1969)].
[18] K. Minematsu and K. Hirakawa, J. Phys. Soc. Jap. **31**, 603 (1971).
[19] R. L. Melcher, Ph. D. thesis (Washington University, St. Louis, Mo., 1968) (unpublished).
[20] L. L. Hess and E. R. Hunt, Phys. Rev. B **6,** 45 (1972).
[21] R. L. Melcher and D. I. Bolef, Phys. Rev. **186,** 491 (1969).
[22] P. A. Fedders, Phys. Rev. B **1,** 3756 (1970).
[23] R. L. Melcher, Phys. Rev. B **1,** 4493 (1970).
[24] D. E. Eastman, Phys. Rev. **156,** 645 (1967).
[25] R. H. Plovnick and S. J. Camobreco, Mater. Res. Bull. **7,** 573 (1972).
[26] R. L. Melcher, D. I. Bolef, and J. B. Merry, Rev. Sci. Instrum. **39,** 1613 (1968).
[27] O. Beckman and K. Knox, Phys. Rev. **121,** 376 (1961).
[28] K. Gesi, J. D. Axe, G. Shirane, and A. Linz, Phys. Rev. B **5,** 1933 (1972).
[29] A. J. Heeger, O. Beckman, and A. M. Portis, Phys. Rev.

123, 1652 (1961).
[30]A. M. Portis and R. H, Lindquist, in *Magnetism*, edited by G. T. Rado and H. Suhl (Academic, New York, 1965), Vol. IIA.
[31]M. F. Thorpe, Phys. Rev. B **2**, 2690 (1970).
[32]R. Weber, Phys. Rev. Lett. **21**, 1260 (1968).

PHYSICAL REVIEW B VOLUME 7, NUMBER 5 1 MARCH 1973

Symmetry Properties of the Transport Coefficients of Magnetic Crystals

A. P. Cracknell
Carnegie Laboratory of Physics, University of Dundee, Dundee DD1 4HN, Scotland, United Kingdom
(Received 27 March 1972)

A discussion of the symmetry properties of tensors describing the transport properties of magnetic crystals, or of nonmagnetic crystals in applied magnetic fields, is given both from the macroscopic and microscopic points of view. A prescription for the simplification of the form of such a tensor is derived (prescription C) which is based on the use of Onsager's theorem and of Neumann's principle both for the unitary symmetry operations and also, in a modified form, for the antiunitary symmetry operations. This is different from the methods used previously by Birss (prescription A) and by Kleiner (prescription B). While prescription A ignores the antiunitary symmetry operations, the use of these operations is included in both prescriptions B and C. However, prescriptions B and C often lead to different results and it is suggested that experiments based on the Hall effect could be used to determine which of these two prescriptions is correct.

I. INTRODUCTION

The reader is assumed to be familiar with the general outlines of the classic book by Nye[1] on the use of symmetry to simplify the forms of tensors describing various physical properties of nonmagnetic crystals.

The first writings in English on the extension of these ideas to the case of crystals exhibiting magnetic ordering are those of Birss,[2,3] based on the quite considerable amount of scattered work of several Russian workers. As far as tensors that describe macroscopic static, or equilibrium, properties are concerned, the treatment given by Birss has found complete acceptance. However, when it comes to the case of transport properties, which describe only quasiequilibrium states or dynamic equilibrium states of a crystal, the tensors involved (the transport coefficients) depend on time, implicitly at least, and there has been some criticism[4–7] of the treatment given by Birss.

In the present paper we shall try to identify the exact nature of the disagreement which has arisen, to establish to what extent it is a matter of semantics or a matter of physics, and to offer some further suggestions on the matter of the symmetry properties of transport coefficients and of any microscopic description of physical phenomena in magnetic crystals.

II. SYMMETRY PROPERTIES OF TENSORS FOR MAGNETIC CRYSTALS—MACROSCOPIC APPROACH

For a nonmagnetic crystal, in the absence of any external magnetic field, there are two separate arguments that can be used to simplify the forms of the tensors representing the transport properties of the crystal (see, for example, Ref. 1). The first is based on the use of Onsager's theorem and the second is based on the use of Neumann's principle. From the use of Onsager's theorem it is possible to show that σ_{ij} and κ_{ij}, the electrical- and thermal-conductivity tensors, are symmetric; that is,

$$\sigma_{ij} = \sigma_{ji} \ , \qquad \kappa_{ij} = \kappa_{ji} \ , \tag{1}$$

and also to obtain a relation between the Peltier tensor π_{ij} and the Seebeck tensor α_{ij}:

$$(1/T)\pi_{ij} = \alpha_{ji} \ . \tag{2}$$

The conditions expressed in Eqs. (1) and (2) apply to any crystal regardless of any crystallographic symmetry that it may possess. The use of Neumann's principle enables one to make use of any crystallographic symmetry to impose further restrictions on the transport coefficients in addition to those given in Eqs. (1) and (2). For any second-rank tensor d_{ij}, Neumann's principle leads to

$$d_{ij} = \sum_p \sum_q R_{ip} R_{jq} d_{pq} \ . \tag{3}$$

In this equation, R_{ip} is the orthogonal matrix that represents the action of a point-group symmetry operation R of the crystal on a vector $\vec{x}_p [= (x_1, x_2, x_3)]$, that is,

$$x_i' = \sum_p R_{ip} x_p \ . \tag{4}$$